
Research Article: New Research | Cognition and Behavior

Dynamics of visual perceptual decision-making in freely behaving mice

<https://doi.org/10.1523/ENEURO.0161-21.2022>

Cite as: eNeuro 2022; 10.1523/ENEURO.0161-21.2022

Received: 13 April 2021

Revised: 14 February 2022

Accepted: 17 February 2022

This Early Release article has been peer-reviewed and accepted, but has not been through the composition and copyediting processes. The final version may differ slightly in style or formatting and will contain links to any extended data.

Alerts: Sign up at www.eneuro.org/alerts to receive customized email alerts when the fully formatted version of this article is published.

Copyright © 2022 You and Mysore

This is an open-access article distributed under the terms of the Creative Commons Attribution 4.0 International license, which permits unrestricted use, distribution and reproduction in any medium provided that the original work is properly attributed.

Dynamics of visual perceptual decision-making in freely behaving mice

2. Abbreviated Title (50 character maximum): Dynamics of visual decision-making in mice

3. Author Names and Affiliations:

Wen-Kai You^{1,2} and Shreesh P. Mysore^{1,2*}

¹Department of Psychological and Brain Sciences, Johns Hopkins University

²The Solomon H. Snyder Department of Neuroscience, Johns Hopkins University

4. Author Contributions: WKY and SPM designed the research and wrote the paper. WKY performed the experiments, and analyzed the data.

5. Correspondence should be addressed to:

Shreesh P. Mysore, PhD

3400 N Charles St, Ames Hall 224

Baltimore MD 21218

mysore@jhu.edu

6. Number of Figures: 5

7. Number of Tables: None

8. Number of Multimedia: None

9. Number of words for Abstract: 242

10. Number of words for Significance Statement: 77

11. Number of words for Introduction: 394

12. Number of words for Discussion: 1973

13. Acknowledgements: We thank James Garmon for help with fabrication of custom equipment.

14. Conflict of Interest: Authors report no conflict of interest.

15. Funding sources: This work was supported by funding from NIH R03 HD093995 and startup funds from Johns Hopkins University.

1
2
3
4
5
6
7
8
9
10
11
12
13
14
15
16
17
18
19
20
21
22
23
24
25
26
27
28
29
30
31
32
33
34
35
36
37
38
39
40
41
42
43
44
45
46
47
48
49
50

Dynamics of visual perceptual decision-making in freely behaving mice

ABSTRACT

Studying the temporal dynamics of perceptual decisions offers key insights into the cognitive processes contributing to it. Conducting such investigation in a genetically tractable animal model can facilitate the subsequent unpacking of the mechanistic basis of different stages in perceptual dynamics. Here, we investigated the time course as well as fundamental psychophysical constants governing visual perceptual decision-making in freely behaving mice. We did so by analyzing response accuracy against reaction time (i.e., conditional accuracy), in a series of 2-AFC orientation discrimination tasks in which we varied target size, luminance, duration, and presence of a foil. Our results quantified two distinct stages in the time course of mouse visual decision-making - a 'sensory encoding' stage, in which conditional accuracy exhibits a classic tradeoff with response speed, and a subsequent 'short term memory (STM)-dependent' stage in which conditional accuracy exhibits a classic asymptotic decay following stimulus offset. We estimated the duration of visual sensory encoding as 200-320 ms across tasks, the lower bound of the duration of short-term memory as ~1700 ms, and the briefest duration of visual stimulus input that is informative as ≤ 50 ms. Separately, by varying stimulus onset delay, we demonstrated that the conditional accuracy function and RT distribution can be independently modulated, and found that the duration for which mice naturally withhold from responding is a quantitative metric of impulsivity. Taken together, our results establish a quantitative foundation for investigating the neural circuit bases of visual decision dynamics in mice.

SIGNIFICANCE STATEMENT

This study presents a quantitative breakdown of the time course of visual decision-making in mice during naturalistic behavior. It demonstrates parallel stages in mouse visual perceptual decision dynamics to those in humans, estimates their durations, and shows that mice are able to discriminate well under challenging visual conditions – with stimuli that are brief, low luminance, and small. These results set the stage for investigating the neural bases of visual perceptual decision dynamics and their dysfunction in mice.

INTRODUCTION

Exploring the temporal dynamics of perceptual decisions from onset of the sensory input through the initiation of behavioral responses affords a key window into the underlying cognitive processes (Uchida, Kepecs et al. 2006, Stanford, Shankar et al. 2010, Siegel, Engel et al. 2011). Investigations of such dynamics in humans (Steinemann, O'Connell et al. 2018, Wilming, Murphy et al. 2020) and other species (Yang, DeWeese et al. 2008, Zariwala, Kepecs et al. 2013, Thura and Cisek 2014) have revealed distinct stages in perceptual processing, their timing, and their interactions. (Wickelgren 1977, McElree and Doshier 1989, Heitz 2014). Performing such investigations in a genetically tractable animal model can additionally facilitate the subsequent unpacking of the mechanistic basis of different stages in perceptual dynamics. However, despite the recent rise in the use of the laboratory mouse for the study of the visual system (Huberman and Niell 2011, Glickfeld, Reid et al. 2014, Seabrook, Burbridge et al. 2017) and of visually guided decision-making (Prusky, West et al. 2000, Prusky and Douglas 2004, Busse, Ayaz et al. 2011, Histed, Carvalho et al. 2012, Carandini and Churchland 2013, Glickfeld, Histed et al. 2013, Long, Jiang et al. 2015, Burgess, Lak et al. 2017, Wang and Krauzlis 2018, Speed, Del Rosario et al. 2020, You and Mysore 2020), the temporal dynamics of visual perceptual decisions represents a significant gap in mouse visual psychophysics (Histed and Maunsell 2014, Umino, Pasquale et al. 2018, Nomura, Ikuta et al. 2019).

In this study, we adapted approaches from human psychophysical studies to investigate the dynamics of visual decision-making in freely behaving mice. In a series of experiments involving touchscreen-based (Mar, Horner et al. 2013, You and Mysore 2020), 2-alternative forced choice (2-AFC) orientation discrimination tasks, we investigated the effect of stimulus size, luminance, duration, delay, and the presence of a competing foil on mouse decision performance (accuracy and reaction time), and importantly,

51 on the conditional accuracy function. We identified two distinct stages in the time course of mouse visual
52 decision-making within a trial, as has been reported in humans (Posner and Keele 1967, Phillips and
53 Baddeley 1971, Dick 1974, Coltheart 1980, Shibuya and Bundesen 1988, Busey and Loftus 1994, Vogel,
54 Woodman et al. 2006, Bays, Gorgoraptis et al. 2011). In the first ‘sensory encoding’ stage (Shibuya and
55 Bundesen 1988, Busey and Loftus 1994, Vogel, Woodman et al. 2006, Bays, Gorgoraptis et al. 2011),
56 response accuracy exhibited a classic tradeoff with response speed, and asymptoted to a peak level. In the
57 next stage, response accuracy did not exhibit such a tradeoff, but instead, decayed following stimulus offset,
58 consistent with a classic short-term memory (STM)-dependent process (Posner and Keele 1967, Phillips
59 and Baddeley 1971, Dick 1974, Coltheart 1980). Combining these results with those from drift diffusion
60 modeling (Ratcliff, Smith et al. 2016) allowed us to estimate fundamental psychophysical constants in
61 mouse perceptual decision-making: the time needed by mice to complete visual sensory encoding, the
62 duration for which their short-term memory can intrinsically support discrimination behavior after stimulus
63 input is removed, and the shortest visual stimulus duration that is informative. Additionally, by varying
64 stimulus onset delay, we demonstrated that the two components of accuracy, namely, the conditional
65 accuracy function and the RT distribution can be independently modulated by task parameters. This also
66 allowed a quantitative estimation of impulsivity of mice. Together, this study reveals parallels between
67 mouse and human visual decision dynamics, despite differences in their sensory apparatuses, and enable
68 investigations into the neural circuit underpinnings of the time course of perceptual decision-making in
69 mice.

70

71 METHODS

72 **Animals.** Thirty-seven mice (33 C57B16/J mice, all male; 4 PV-Cre mice, 3 female, Jackson Labs) were
73 housed in a temperature (~75F) and humidity (~55%) controlled facility on a 12:12h light:dark cycle;
74 ZT0=7 am. All procedures followed the NIH guidelines and were approved by the [Author Institutions]
75 Animal Care and Use Committee (ACUC). Animals were allowed to acclimate for at least one week, with
76 *ad libitum* access to food and water before water regulation was initiated per previously published
77 procedures (Guo, Hires et al. 2014). Briefly, mice were individually housed (for monitoring and control of
78 daily water intake of each identified animal), and administered 1mL water per day to taper their body weight
79 down, over the course of 5-7 days, to 80-85% of each animal’s free-feeding baseline weight. During
80 behavioral training/testing, the primary source of water for mice was as a reinforcer for correct performance:
81 10 μ L of water was provided for every correct response. Experiments were all carried out in the light phase.

82

83 **Apparatus.** Behavioral training and testing were performed in soundproof operant chambers equipped with
84 a touchscreen (Med Associates Inc.), a custom-built reward port (fluid well), infrared video cameras, a
85 house light and a magazine light above the reward port. The reward port was located at the opposite wall
86 of the chamber relative to the touchscreen (Fig. 1A, 1-1A). Mice were placed within a clear plexiglass tube
87 (5cm diameter) that connects the touchscreen and the reward port. A thin plexiglass mask (3 mm thickness)
88 was placed 3 mm in front of the touchscreen with three apertures (1cm diameter) through which mouse was
89 allowed to interact with the screen via nose-touch. The ‘left’ and ‘right’ apertures were placed 3cm apart
90 (center-to-center) along the base of the triangle, and a ‘central’ aperture, at the apex of the triangle, was 1.5
91 cm below the midpoint of the base. All experimental procedures were executed using control software (K-
92 limbic, Med-Associates).

93

94 **Visual stimuli.** Visual stimuli were bright objects on the dark background (luminance = 1.32 cd/m^2). A
95 small cross (60x60 pixels; luminance = 130 cd/m^2) was presented in the central aperture and had to be
96 touched to initiate each trial. Oriented gratings (horizontal or vertical) were generated using a square wave,
97 with fixed spatial frequency (24 pixels/cycle) known to be effective for mice to discriminate (Histed,
98 Carvalho et al. 2012). The dark phase of the grating was black, identical to the background (luminance,
99 $L_{\text{dark}} = 1.32 \text{ cd}/\text{m}^2$), and the bright phase was varied between 1.73 cd/m^2 and 130 cd/m^2 depending on the
100 tasks (see below). (Note that as the luminance of the bright phase of the grating changed, the contrast of the
101 grating also changed. For clarity, we refer to this stimulus manipulation as a change in luminance,

102 throughout.) The size of the stimulus was also varied depending on the task, ranging from 60 pixels x 60
103 pixels to 108 pixels x 108 pixels, which subtended 25-45 visual degrees at a viewing distance of 2 cm from
104 the screen (Fig. 1-1A).

105
106 **Experimental procedure and behavioral training.** Each mouse was run for one 30 min behavioral session
107 per day, with each session yielding 80-180 trials. Each trial in a session was initiated by the mouse touching
108 the zeroing cross. Upon trial initiation, the cross vanished, and the visual stimulus (or stimuli) were
109 immediately presented (except in the delay task), for a duration of 0.1-3s depending on the task (see below).
110 Mice were trained to report the orientation of target grating, by nose-touching the correct response aperture
111 (vertical → left; horizontal → right). A correct response triggered a tone (600 Hz, 1 sec), the magazine light
112 turning on, and the delivery of 10 μ L of water. When mice turned to consumed the reward, their head entry
113 into the reward port was detected by an infrared sensor which caused the zeroing cross (for the next trial)
114 to be presented again. An incorrect response triggered a 5-s timeout, during which the house light and the
115 magazine light were both on and zeroing cross was unavailable for the next trial to be initiated. A failure to
116 respond within 3s (starting stimulus presentation) resulted in a trial reset: the stimulus vanished and the
117 zeroing cross was presented immediately (without a timeout penalty), to allow initiation of the next trial.
118 Well-trained animals failed to respond on fewer than 5% of the total number of trials, and there were no
119 systematic differences in the proportion of such missed trials between different conditions. Within each
120 daily 30-minute behavioral session, mice consumed approximately 1mL of water. If a mouse failed to
121 collect enough water from the behavioral session, they were provided with a water supplement using a
122 small plastic dish in their home cage.

123
124 **Single-stimulus discrimination task.** Upon trial initiation, a single grating stimulus (i.e., the ‘target’) was
125 presented above the central aperture, at the same horizontal level as the left and right apertures, and mice
126 were required to report its orientation with the appropriate nose-touch (Fig. 1B). When stimulus size and
127 luminance were manipulated (Fig. 1, and 2), three different sizes were tested: 60x60, 84x84, 108x108
128 (pixels x pixels). For each size, seven different levels of luminance were tested: 2.00, 2.59, 4.37, 7.55, 16.2,
129 34.3, 130 cd/m². (These corresponded nominally to Michelson’s contrasts of 20%, 32%, 54%, 70%, 85%,
130 93%, 98%, respectively; Michelson’s contrast is computed as $(\text{luminance}_{\text{bright}} - \text{luminance}_{\text{dark}}) /$
131 $(\text{luminance}_{\text{bright}} + \text{luminance}_{\text{dark}}) * 100$.) Trials with different stimulus luminance at a particular size were
132 interleaved randomly throughout a session, while trials with different stimulus sizes were examined on
133 different days. When the stimulus duration was manipulated (Fig. 3), the luminance (130 cd/m²) and size
134 (60 pix x 60 pix) of the grating were fixed, and eleven different stimulus durations were tested: 100 ms,
135 200, 300, 400, 500, 600, 800, 1000, 1500, 2000, 3000 ms. The stimulus duration was fixed for a given day,
136 and across days, was varied in a descending sequence from 3000 ms to 100 ms. When the stimulus onset
137 delay was manipulated (Fig. 5), the luminance (130 cd/m²), size (60 pix x 60 pix), and duration (600 ms)
138 of the grating were fixed. Three different delays were tested: 0, 100, and 200 ms. The delay duration was
139 fixed for a given day, and varied in an ascending sequence from 0 ms to 200 ms.

140
141 **Flanker task.** Upon trial initiation, either one stimulus (‘target’, 60 pix x 60 pix, luminance = 20.1 cd/m²)
142 was presented at the lower location, or two stimuli were presented simultaneously, with the target at the
143 lower location and a second ‘flanker’ at the upper location (Fig.4A). Flankers were of the same size (60 pix
144 x 60 pix) and spatial frequency (24 pixel/cycle) as the target, but with luminance ranging (over 8 levels)
145 from less than that of the target to greater than that of the target (You and Mysore 2020). The orientation
146 of the flanker was either identical to that of the target (‘congruent trial’) or orthogonal to that of the target
147 (‘incongruent trial’). The stimulus (stimuli) was (were) presented for a duration of 1s, and mice were
148 required to report orientation of the target grating with the appropriate nose-touch (within 3s). All types of
149 trials (no flanker, congruent, incongruent) and flanker luminance were interleaved randomly within each
150 daily session. Data from this experiment have been reported previously (You and Mysore 2020), and were
151 re-analyzed here using different analyses.

152

153 **Subject inclusion/exclusion.** A total of 37 mice were used in this study, with different subsets used in
154 different tasks. For mice involved in more than one task, they were well-rested for 3-8 weeks with food and
155 water *ad libitum* between experiments. Before the start of each experiment, all mice were given a few days
156 of practice session to ensure that they remembered/re-learned the association between the orientation of
157 single target and the appropriate nose-touch. Of the total of 37 mice trained across tasks, 28 mice passed
158 the inclusion threshold of response accuracy >70% in the single stimulus discrimination task, and were
159 included for the analyses reported in this paper.

160
161 **Trial inclusion/exclusion.** Mice were observed to become less engaged in the task towards the end of a
162 behavioral session, when they had received a sizeable proportion of their daily water intake. This was
163 reflected in their behavioral metrics: they tended to wait longer to initiate the next trial, and their
164 performance deteriorated. We identified and excluded such trials following a published procedure (You
165 and Mysore 2020), in order to minimize confounds arising from loss of motivation towards the end of
166 sessions. Briefly, we pooled data across all mice and all sessions, treating them as coming from one session
167 of a single ‘mouse’. We then binned the data by trial number within the session, computed the
168 discrimination accuracy in each bin (% correct), and plotted it as a function of trial number within session
169 (Fig. 1-1B, 3-1A, 5-1A). Using a bootstrapping approach, we computed the 95% confidence interval for
170 this value. We used the following exclusion criterion: Trials q and above were dropped if the q^{th} trial was
171 the first trial at which *at least one* of the following two conditions was satisfied: (a) the performance was
172 statistically indistinguishable from chance on the q^{th} trial and for the majority (3/5) of the next 5 trials
173 (including the q^{th}), (b) the number of observations in q^{th} trial was below 25% of the maximum possible
174 number of observations for each trial (Σ mice*sessions), thereby signaling substantially reduced statistical
175 power available to reliably compare performance to chance. The plots of performance as a function of trial
176 number, and number of observations as a function of trial number for the different tasks in this study are
177 shown in Figs. 1-1B, 3-1A, 5-1A, along with the identified cut-off trial numbers (q).

178
179 **Behavioral measurements:** Response accuracy (% correct) was calculated as the number of correct trials
180 divided by the total number of trials responded (correct plus incorrect). Reaction time (RT) was defined as
181 the time between the start of stimulus presentation and time of response nose-touch, both detected by the
182 touchscreen. In the experiment involving stimulus onset delays (Fig. 5A), RT was computed with respect
183 to trial initiation (as opposed to from stimulus onset).

184
185 **Drift diffusion modeling of RT distributions.** The RT measured here represents the duration from
186 stimulus onset to completion of execution of the motor response. In order to specifically isolate the time
187 spent in decision making (separately from the latency of activation of sensory neurons as well as duration
188 of motor execution), we applied the drift-diffusion model to our RT data (Voss, Nagler et al. 2013, Voss,
189 Voss et al. 2015). This model hypothesizes that a subject (‘decision maker’) collects information from the
190 sensory stimulus via sequential sampling, causing sensory evidence to accrue for or against a particular
191 option (usually binary) while viewing the stimulus. A decision is to be made when the accumulating
192 evidence reaches an internal threshold of the subject. This process of evidence accumulation, together with
193 the processes of sensory encoding and motor execution, as well as threshold crossing, determine the RT
194 observed on each trial.

195 We used a standard version of the model that consists of four independent variables (Ratcliff 1978,
196 Ratcliff, Smith et al. 2016): (1) the drift rate, (2) the boundary separation, (3) the starting point, and a (4)
197 non-decisional constant (t_{delay}), which accounts for the time spent in sensory encoding and motor execution.
198 In the case of our tasks, there was no reason for the drift rate to be different between vertical versus
199 horizontal gratings, and therefore, we merged both type of trials (trials with a horizontal target grating and
200 trials with a vertical target grating). We treated ‘correct’ response and ‘incorrect’ response as the two binary
201 options, and fit the diffusion model to the RT distributions of correct versus incorrect trials using the fast-
202 dm-30 toolbox with the maximum likelihood option to gain estimates of those four parameters for each
203 individual mouse (Fig. 2-2)(Voss, Voss et al. 2015).

204

205 **Conditional accuracy analysis.** Conditional accuracy was calculated as the percentage of correct trials
 206 (accuracy) as a function of RT. For this analysis, trials from all mice were pooled together and treated as if
 207 they were from one single mouse for statistical power (Fig. 2 onwards; for completeness, conditional
 208 accuracy plots using non-pooled data, i.e., from individual mice, are included in Extended Figures). Pooled
 209 trials were then sorted by their RT, and then binned by RT such that there were: (1) sufficient number of
 210 trials in each bin; and (2) sufficient number of total bins, to ensure the robustness of curve fitting and
 211 therefore the estimates of quantitative metrics (see below). Typical bin sizes used were 50ms, 100 ms or
 212 200 ms bins, depending on the experiments and stage of analysis (sensory encoding or STM-dependent).
 213 The effect of bin size on the estimates of quantitative metrics is explored in the Extended Figures; results
 214 show that the estimates are comparable across tested bin sizes.

215

216 **Conditional accuracy function (CAF).** To quantitatively describe the relationship between the conditional
 217 accuracy and RT, we fitted the plot of accuracy against binned RT with parametric functions (the CAF; see
 218 below) using a nonlinear least square method. For RT bins aligned to stimulus onset (Fig. 2, 4C, 5B), we
 219 fit the conditional accuracy data using an increasing asymptotic function:

220

221

222

$$\text{Conditional accuracy} = \lambda (1 - e^{-\gamma_{enc} (RT - \delta)}).$$

223

224 Three key metrics were defined for this sensory encoding phase, for use in subsequent comparisons
 225 across conditions: (1) peak conditional accuracy (a_{peak}), the maximal level of accuracy that the CAF reaches
 226 within the range of RT; (2) the slope parameter (γ_{enc}); and (3) the first instant at which the conditional
 227 accuracy reaches its maximal value (t_{peak}) - defined as the time point at which the ascending CAF reaches
 228 95% of a_{peak} . Note that t_{peak} is influenced by the peak conditional accuracy (a_{peak}), the slope parameter, γ_{enc} ,
 229 and the temporal offset at chance performance, δ . For RT bins aligned to stimulus offset (Fig. 3C, 4E, 5D),
 we fit the decaying conditional accuracy data using a sigmoidal function:

230

231

232

$$\text{Conditional accuracy} = \lambda [1 / (1 + e^{-\beta_{dec} (RT - \tau)})] + 50$$

233

234 Three key metrics were defined for this STM-dependent stage for use in subsequent comparisons across
 235 conditions: (1) peak conditional accuracy (a_{peak}), the maximal level of accuracy within the range of RT; (2)
 236 the first instant (t_{decay}) at which conditional accuracy is lower than the maximum - defined as the time point
 237 at which the descending CAF crosses 95% of a_{peak} ; and (3) the first instant (t_{chance}) at which conditional
 238 accuracy drops to chance levels - defined as the timepoint at which the descending CAF crosses 52.5%. In
 239 (rare) cases when the CAF never went below 52.5%, t_{chance} was set to be the upper bound of the window of
 240 analysis (i.e., 3000ms - stimulus duration = the window for which the mice can respond following stimulus
 offset). Note that t_{decay} and t_{chance} are influenced by both the slope parameter, β_{dec} , and τ .

241

242 Confidence intervals of the CAF fits, as well as for the parameters, were estimated by standard
 243 bootstrapping procedures involving resampling the raw data randomly with replacement (1000 x), to get
 244 repeated estimates of the CAF and corresponding metrics. In all relevant figures, the box plots of the
 245 estimated values of each metric show the median (the central mark), the 25th and 75th percentiles (the
 bottom and top edge of the box), and the most extreme data points not considered as outliers (whiskers).

246

247 In the experiment in which the stimulus onset delay was manipulated (Fig. 5), we adopted the following
 248 two adjustments to our procedure for the analysis of the conditional accuracy function. First, since the
 249 stimulus was short (600 ms), in order to ensure robust estimates of CAF metrics for the sensory encoding
 250 stage, we included data beyond stimulus offset as well for the fitting of the CAF through 400 ms following
 251 offset. (We chose to include data upto 400 ms after offset, specifically, because we had learned from Figure
 252 3 that conditional accuracy remains at its plateau for nearly 500 ms following stimulus offset.) Second, we
 253 also excluded trials with RT < 200ms for the fitting of the CAF (Fig. 5B), because these represent trials on
 254 which responses were initiated prematurely (200 ms represents our estimate of the duration of sensory
 latency plus motor execution; see text surrounding Figure 2).

255

256

257

258

259

260

261

262

263

264

265

266

267

268

269

270

271

272

273

274

275

276

277

278

279

280

281

282

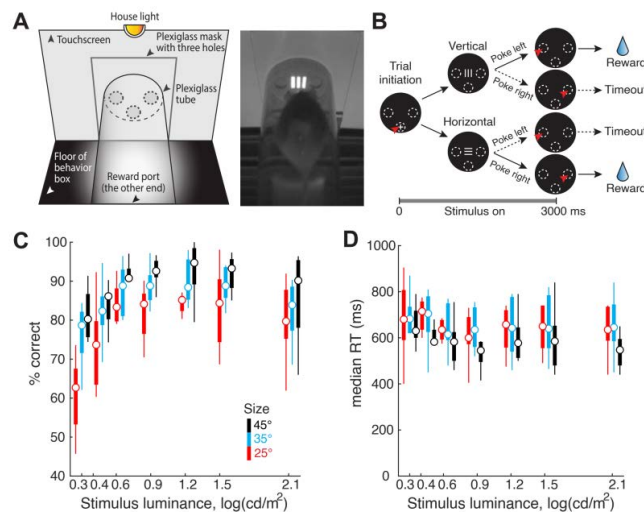
283

Statistical tests. All analyses and statistical tests were performed in MATLAB. For single-stimulus experiments in which only one stimulus parameter was systemically varied, one-way ANOVA was applied to examine the effect of the manipulating the single factor (duration and delay, Fig. 3AB, 5A, 1-1CD). For experiments that involved changing both stimulus size and luminance (Fig. 1CDE, 2-2), two-way ANOVA was applied to examine the effect of each factor, as well as their interaction. For the flanker task, the paired-sample t-test was used to examine if the group performance was different between trial types (Fig. 4B).

For the metrics associated with CAF, comparisons were made by measuring the effect size (Hedges' g) of the difference between two distributions (Fig. 2BD, 4DF and 5CE). All effect size measurements, including those with ANOVA (η^2), were calculated following the methods (and source code) of Hentschke and Stüttgen (2011)(Hentschke and Stüttgen 2011). Hedges' g estimates the distance between the two distributions in units of their pooled standard deviation, with larger numbers indicating stronger effects. η^2 varies from 0 to 1, with larger values indicating greater ratio of variance explained in the dependent variable by a predictor while controlling the other variables.

RESULTS

In this study, freely behaving mice were trained to perform 2-AFC orientation discrimination in a touchscreen-based setup (Mar, Horner et al. 2013, You and Mysore 2020)(Methods). Briefly, mice were placed in a plexiglass tube within a soundproof operant chamber equipped with a touch-sensitive screen at one wall and a reward well at the opposite wall (Fig. 1A). A plexiglass sheet with three holes was placed in front of the touchscreen - the holes corresponded to the locations at which mice were allowed to interact with the screen by a nose-touch (Fig. 1A). All trials began with a nose-touch on a bright zeroing-cross presented within the lower central hole (Fig. 1B). Immediately following nose-touch, an oriented grating (target; bright stimulus on a dark background) was presented at the center of the screen. Mice were rewarded if they responded to the orientation of the target with an appropriate nose-touch: vertical (horizontal) grating \rightarrow touch within upper left (upper right) hole. Behavioral data were collected from daily sessions that lasted 30 minutes for each mouse.



284

285

286

287

288

Figure 1. Stimulus luminance and size modulate orientation discrimination performance in freely behaving mice. (A) Left: Schematic of touchscreen-based experimental setup showing key components. Right: Snapshot of freely behaving mouse facing a visual stimulus on the touchscreen. (B) Schematic of 2-AFC task design. Black discs: Screenshots of touchscreen with visual stimuli; dashed ovals: locations of holes through which mice can interact with

289 touchscreen; white '+': zeroing cross presented within central response hole at start of each trial; red arrowhead: nose-
 290 touch by mouse. Shown also are vertical or horizontal grating stimuli, and reinforcement (water)/punishment (timeout)
 291 schedule. **Bottom**: Trial timeline. 0 ms corresponds to the instant at which the mouse touches the zeroing cross (trial
 292 initiation). Immediately following this, the target grating was presented and stayed on for 3s, or until the mouse
 293 responded, whichever came first. Vertical and horizontal targets were interleaved randomly. **(C)** Psychometric plots
 294 of discrimination accuracy against stimulus luminance (n=8 mice). Different colors correspond to different target sizes.
 295 2-way ANOVA, $p < 0.001$ (luminance), $p < 0.001$ (size), $p = 0.498$ (interaction). Effect size $\eta^2 = 0.292$ (luminance),
 296 $\eta^2 = 0.192$ (size), $\eta^2 = 0.037$ (interaction). For each stimulus size/luminance, the box plot shows the median (the central
 297 mark), and the 25th and 75th percentiles (the bottom and top edge of the box) of the group (n=8). The whiskers extend
 298 to the most extreme data points not considered as outliers. **(D)** Plot of median reaction time (RT) against stimulus
 299 luminance. 2-way ANOVA, $p = 0.998$ (luminance), $p = 0.004$ (size), $p = 1$ (interaction). Effect size $\eta^2 = 0.003$ (luminance),
 300 $\eta^2 = 0.071$ (size), $\eta^2 = 0.010$ (interaction).

301 **See also Fig. 1-1.**

302

303 **Stimulus size and luminance modulate mouse discrimination performance**

304 We first examined the effect of target size and luminance on the decision performance of mice in the
 305 orientation discrimination task. Here, the target grating was presented for up to 3 seconds after trial initiation
 306 (Fig. 1B; Methods), and its size and luminance were systematically varied; the spatial frequency was fixed
 307 at 0.1 cycles/degree (24 pixels/cycle) (Prusky and Douglas 2004, Histed, Carvalho et al. 2012) (Methods).
 308 Mice were allowed to respond at any time during stimulus presentation, and the stimulus was terminated
 309 automatically upon response.

310

311 We found that both the target luminance and size significantly modulated discrimination accuracy (Fig. 1C,
 312 2-way ANOVA, main effect of luminance, $p < 0.001$, effect size $\eta^2 = 0.292$; main effect of size, $p < 0.001$,
 313 $\eta^2 = 0.192$; interaction, $p = 0.498$, $\eta^2 = 0.037$). These results revealed that mice discriminated target orientation
 314 better than chance even at the lowest luminance (2.00 cd/m²) and size (25°) tested (Fig. 1C; the red box at
 315 the left lower corner, $p = 0.015$, *t*-test against mean accuracy=50%, effect size $g = 1.129$). Additionally, at
 316 this smallest target size (25°), mice could discriminate with >80% accuracy for most of the tested luminance
 317 values (≥ 4.37 cd/m²; Fig. 1CD, red data).

318

319 The effect of these parameters on median reaction times (RTs) was less pronounced. Target size, but not
 320 luminance, modulated reaction times (RTs) (Fig. 1E, two-way ANOVA; main effect of size, $p = 0.004$, effect
 321 size $\eta^2 = 0.071$; main effect of luminance, $p = 0.998$, $\eta^2 = 0.003$; interaction, $p = 1$, $\eta^2 = 0.010$). Together, these
 322 results revealed a systematic effect of target size and luminance on discrimination accuracy.

323

324

325 **Effect of stimulus size and luminance on dynamics of visual decision-making: the sensory encoding** 326 **stage**

327 To investigate the dynamics of visual perceptual decision-making, we adapted approaches from human
 328 studies and examined the dependence of response accuracy on RT, i.e., the so-called 'conditional accuracy'
 329 function (CAF) (Wickelgren 1977, McElree and Doshier 1989, Heitz 2014). For these analyses, we pooled
 330 trials from all mice (n=8) in order to gain better statistical power for the estimates of parameters of the CAF
 331 (Methods; plots of the data for individual mice showed similar overall shapes of the CAF; Fig. 2-1A).

332

333 Specifically, we investigated the dynamics of visual perceptual decision-making as a function of stimulus
 334 size, and separately, as a function of stimulus luminance. First, to examine the effect of stimulus size on
 335 decision dynamics, we pooled trials from all mice across luminance values (7 luminance values) for each
 336 stimulus size, sorted them based on RT, and plotted conditional accuracy for each RT bin (100ms; Fig. 2A;
 337 Methods). We found that for responses with RT less than ~500 ms, conditional accuracy improved for
 338 longer RT, consistent with the classic 'speed-accuracy tradeoff' [34]. For responses with RT greater than
 339 500 ms and up to 3s, the allowed duration for responses, conditional accuracy plateaued, and was
 340 independent of RT. Next, to examine the effect of stimulus luminance on decision dynamics, we pooled

341 trials from all mice across size values into two groups based on stimulus luminance: (1) trials with target
 342 luminance ≤ 4.37 cd/m² ('low luminance'), and (2) trials with target luminance > 4.37 cd/m² ('high
 343 luminance'; Methods). Here, as well, we found a similar initial stage of increasing conditional accuracy
 344 upto RT of ~ 500 ms, followed by a plateauing of conditional accuracy.

345
 346 Drawing upon arguments from human behavioral studies, we reasoned that the initial transient stage of the
 347 conditional accuracy function reflects the process of sensory encoding: during it, slower responses allow
 348 more sensory evidence to be acquired, thereby improving conditional accuracy up to a peak value reflecting
 349 the completion of sensory encoding (Shibuya and Bundesen 1988, Busey and Loftus 1994, Vogel,
 350 Woodman et al. 2006, Bays, Gorgoraptis et al. 2011).

351
 352 To quantify these dynamics, we fit the conditional accuracy data with an asymptotic function (Fig. 2AC,
 353 solid curves) (Wickelgren 1977, McElree and Doshier 1989, Heitz 2014), and estimated three key metrics,
 354 in each case: (1) the peak conditional accuracy (a_{peak}), (2) the slope parameter (γ_{enc}), and (3) the timepoint
 355 at which conditional accuracy reached its peak (t_{peak} ; Methods).

356
 357 We found that the peak conditional accuracy was significantly modulated by stimulus size (Fig.2B-left;
 358 a_{peak} : size 25° = 81.3 [79.1, 83.7] %; size 35° = 88.0 [86.5, 89.4] %; size 45° = 92.4 [90.7,
 359 94.1] %; effect size Hedge's $g = -6.71$ (25°-35°), -5.39 (35°-45°), -10.6 (25°-45°)), but not the slope of the
 360 function (slope parameter, γ_{enc} , Fig. 2B-middle, size 25° = 6.52 [5.10, 9.07] a.u.; size 35° = 8.81 [7.09,
 361 10.6] a.u.; size 45° = 7.92 [6.15, 10.1] a.u. Hedges' $g = -2.24$ (25°-35°), 0.863 (35°-45°), -1.34 (25°-45°)),
 362 or the time to reach peak accuracy (t_{peak} , Fig. 2B-right, size 25° = 493 [375, 597] ms; size 35° = 459 [420,
 363 505] ms, size 45° = 466 [420, 522] ms; Hedges' $g = 0.728$ (25°-35°), -0.274 (35°-45°), 0.558 (25°-45°)).

364
 365 Next, we found that the peak conditional accuracy was higher in high-luminance trials (Fig. 2D-left, low-
 366 luminance, median [C.I.] = 84.7 [82.7, 86.3] %; high-luminance = 89.5 [88.2, 90.7] %, effect size Hedges'
 367 $g = -6.13$). The slope was also higher in high-luminance trials (slope parameter, γ_{enc} , Fig. 2D-middle, low-
 368 luminance = 6.37 [5.21, 7.78] a.u.; high-luminance = 10.32 [8.49, 12.6] a.u., Hedges' $g = -4.51$) suggesting
 369 a faster rate of sensory encoding in high-luminance trials. Consistent with this, the time to reach peak
 370 accuracy was shorter in high-luminance trials (Fig.2D-right; t_{peak} : low-luminance = 531 [478, 599] ms; high-
 371 luminance = 412 [378, 448] ms, Hedges' $g = 4.86$).

372
 373 The RT measured here represents the duration from the start of the sensory input to the completion of motor
 374 response. In order to obtain an estimate of the duration, specifically, of decision-making, we employed the
 375 standard drift diffusion modeling (DDM) approach (Ratcliff 1978, Ratcliff, Smith et al. 2016) (Methods).
 376 Briefly, the DDM analyzes the full RT distribution and yields a quantitative estimate of four parameters
 377 (Methods), one of which is t_{delay} , a parameter which accounts for the combination of: (a) the time taken for
 378 the sensory (visual) periphery to transduce and relay information to visual brain areas (i.e., neural response
 379 latency), as well as (b) the time taken for executing the motor response (i.e., motor execution delay). In our
 380 tasks, the latter corresponds to the time for the mouse to move its head (and body) to achieve the appropriate
 381 nose-touch.

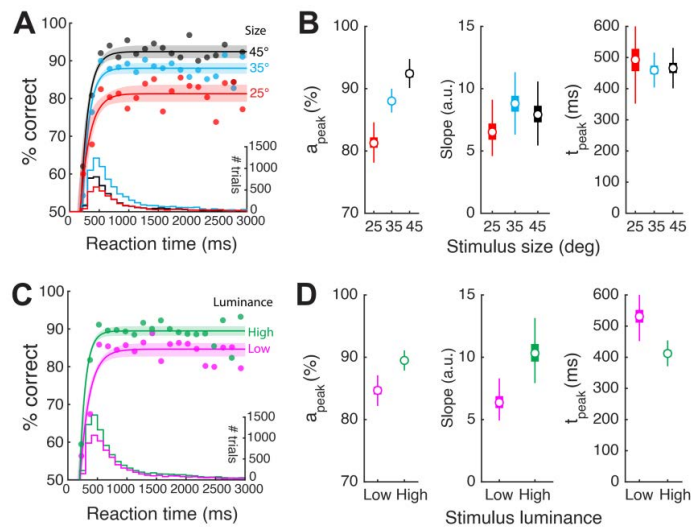
382
 383 Using this approach, we found that stimulus size as well as luminance had no discernable effect on t_{delay}
 384 (Fig. 2-2. 2-way ANOVA, size: $p=0.308$, luminance: $p=0.523$; interaction: $p=0.931$), and the average value
 385 of t_{delay} was 212 ms. Consequently, we estimated the duration of just the sensory encoding stage (temporal
 386 integration window) as $t_{peak} - t_{delay} = t_{peak} - 212$ ms. Across conditions, this took values of 200 ms (412 ms
 387 -212 ms; high luminance), 254 ms (466-212 ms; size of 45 deg), 247 ms (459-212 ms; size of 35 deg), 281
 388 ms (493-212 ms; size of 25 deg), and 319 ms (531 ms -212 ms, low luminance).

389

390 Thus, conditional accuracy analysis allowed us to quantify the sensory encoding stage in mouse visual
 391 perceptual dynamics. We estimated its duration to be brief, varying between 200 ms and 320 ms across the
 392 tested conditions.

393
 394 Following the completion of sensory encoding, a fully constructed representation of the sensory stimulus
 395 is available, as a result of which, additional sampling of the stimulus brings no extra benefits to the
 396 performance. Our finding that RTs longer than t_{peak} produce no further increase in conditional accuracy, is
 397 consistent with the view (Fig. 2AC).

399



400

401 **Figure 2. Stimulus size and luminance modulate the sensory encoding stage of the conditional accuracy function**
 402 **(CAF).** (A) Plot of accuracy as a function of RT bins (conditional accuracy) using same dataset as Fig. 1. Data pooled
 403 across all stimulus luminance and mice ($n=8$), sorted by stimulus size; RT bin size = 100 ms. Solid curves: Conditional
 404 accuracy functions (CAFs, best-fit rising asymptotic function; Methods) for targets of different sizes (black: 45°; blue:
 405 35°; red: 25°); light shading: 95% CI of the fit (Methods). Histograms at bottom: RT distributions for targets of
 406 different sizes (y-axis on the right). The overall response accuracy for a particular stimulus condition is the dot product
 407 of the CAF and the RT distribution. (B) Box plots of the key parameters for different target sizes. Left panel: a_{peak} ;
 408 middle panel: slope parameter; right panel: t_{peak} . (C) CAFs for targets of different luminance conditions (magenta:
 409 'low' luminance - first three luminance levels from Fig. 1C; green: 'high' luminance - last four luminance levels;
 410 Methods); conventions as in A. (D) Box plots of the key parameters for different luminance conditions; conventions
 411 as in C. The box plots in all panels show the median (open circle), the 25th and 75th percentiles (the bottom and top
 412 edge of the box), and the most extreme data points not considered as outliers (whiskers); in some panels, the boxes
 413 are the same size as the symbol for the median.

414 See also Fig. 2-1, 2-2.

415

416

417 Stimulus duration and the dynamics of visual decision-making: the memory-dependent stage

418 The next stage in the time course of perceptual decisions has been identified in human studies as the so-
 419 called 'short-term memory' (STM)-dependent stage, during which an internal representation of the sensory
 420 stimulus is available transiently in memory for guiding behavior (Smith and Ratcliff 2009). Studies have
 421 demonstrated the STM to be labile such that once the stimulus is terminated, sensory information
 422 maintained in STM decays and is lost (over seconds) (Brown 1958, Gold, Murray et al. 2005, Zhang and
 423 Luck 2009, Barrouillet and Camos 2012, Ricker, Vergauwe et al. 2016).

424

425

426

427

428

429

430

431

432

433

434

435

436

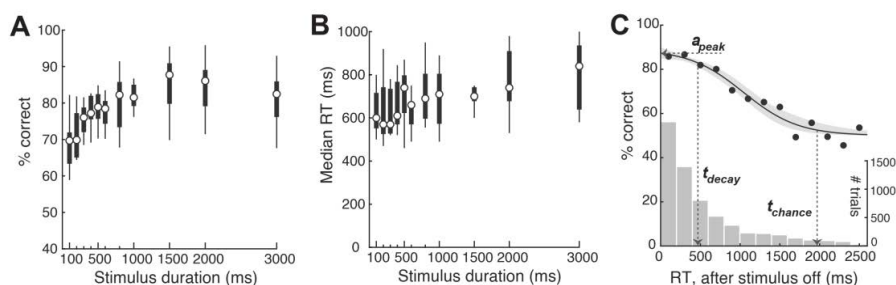
437

438

439

In our experiments so far, the target stimulus was present on the screen for the full duration of the response window (3s). Here, in order to investigate and quantify the STM-dependent stage of mouse perceptual decisions, we performed an experiment in which we shortened the stimulus duration systematically from 3s to 100 ms. This allowed us to examine the time course of decision behavior following stimulus offset, and, as well, to examine the shortest stimulus that mice are able to discriminate effectively.

We first examined overall mouse behavioral performance at different stimulus durations. We found that response accuracy was significantly modulated (Fig.3A, one-way ANOVA, $p < 0.001$, effect size $\eta^2 = 0.331$), with accuracy decreasing for shorter stimulus durations (Pearson's $\rho = 0.712$, $p = 0.014$). There was also a trend of decreasing median RT for shorter stimulus durations (Fig.3B, one-way ANOVA, $p = 0.056$, effect size $\eta^2 = 0.177$; Pearson's $\rho = 0.861$, $p = 0.001$). Additionally, these results revealed, that the shortest stimulus duration needed for mice to be able to discriminate above chance was less than 100 ms - the smallest duration tested (Fig. 3B).



440

441

442

443

444

445

446

447

448

449

450

451

Figure 3. Stimulus duration and the memory-dependent stage of the conditional accuracy function.

(A) Psychometric plot of discrimination accuracy against stimulus duration ($n = 9$ mice; 1-way ANOVA; $p < 0.001$, effect size $\eta^2 = 0.331$). (B) Plot of median reaction time (RT) against stimulus duration (1-way ANOVA; $p = 0.056$, effect size $\eta^2 = 0.177$). (C) Plot of the conditional accuracy (solid data) as a function of RT bins relative to stimulus offset. Only trials in which the stimulus was longer than 332 ms were included (in order to ensure full sensory encoding - see text; Methods). Curve and shading: best-fit sigmoid function and 95% C.I. Bootstrapped estimates of each key metric: a_{peak} , median [C.I.] = 87.3 [84.8, 89.9] %; $t_{decay} = 469$ [279, 697] ms; and $t_{chance} = 1969$ [1708, 2520] ms. Histogram: RT distribution (y axis on the right). In this experiment, stimulus size and luminance were maintained fixed at 25° and 130 cd/m^2 respectively.

See also Fig. 3-1.

452

453

454

455

456

457

458

459

460

461

462

463

464

465

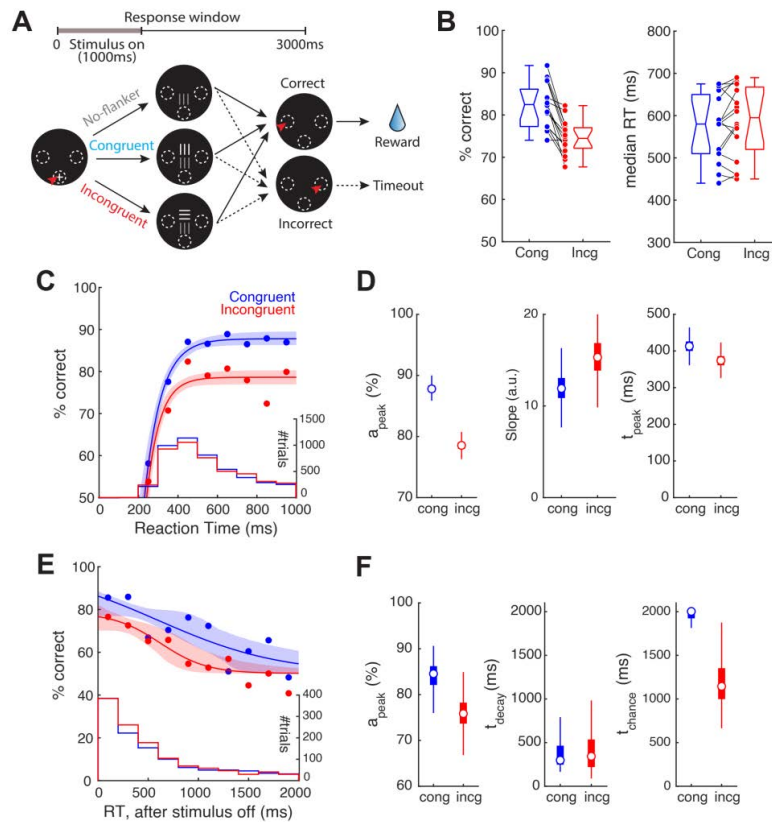
Next, to examine the decision dynamics following stimulus offset, we aligned trials to stimulus offset, and computed the conditional accuracy. Considering that incomplete sensory encoding may be a confounding factor to the STM decay, we only included those trials on which the stimulus was presented for longer than the duration of the sensory encoding stage, estimated in Figure 2 to be 320 ms.

We observed the classic decay in conditional accuracy with longer RTs (Fig. 3C). To quantify the time course of the decay, we fit the conditional accuracy data with a sigmoidal function (Methods), and estimated three key metrics (Fig. 3C; Methods). The first, peak performance, a_{peak} , was 87.3% (median, C.I. = [84.8, 89.9] %), comparable to the asymptotic level of Figure 2, thereby supporting that sensory encoding is, indeed, complete on these trials. The second, the time point at which the conditional accuracy dropped below the peak value, t_{decay} , was 469 ms (median, C.I. = [279, 697] ms) after stimulus offset. The third, the first timepoint at which the discrimination accuracy dropped to a level indistinguishable from the chance, t_{chance} , was 1969 ms (median, C.I. = [1708, 2520] ms) after stimulus offset (Methods).

466 Thus, our conditional accuracy analysis allowed us to investigate quantitatively the second, STM-dependent
 467 stage in mouse visual perceptual dynamics. We estimated the duration over which above-chance decision
 468 accuracy is supported in mice after stimulus offset as ~ 1700 ms (i.e., t_{chance} minus the t_{delay}).
 469
 470

471 The presence of flanker stimulus modulates perceptual dynamics

472 We next investigated the impact of sensory context on visual decision dynamics. It is well-established that
 473 the sensory context in which the perceptual target is presented modulates animals' behavior (Miller 1991,
 474 Meier, Flister et al. 2011, Whitney and Levi 2011). For instance, in the classic flanker task in humans,
 475 the co-occurrence of a flanker stimulus with conflicting information can interfere with perceptual performance
 476 (Eriksen and Eriksen 1974, Fan, McCandliss et al. 2002). Recently, similar results were demonstrated in
 477 mice using a touchscreen version of the flanker task (You and Mysore 2020). In this task (Fig. 4A), a target
 478 grating (always presented at the lower location) was accompanied by a flanker grating at the upper location
 479 with either orthogonal orientation ('incongruent' flanker) or same orientation ('congruent' flanker).
 480 Compared to the presence of a congruent flanker, the 'incongruent' flanker significantly impaired
 481 discrimination accuracy (Fig. 4B-left; $p < 0.001$, paired-sample t test, effect size Hedges' $g = 1.61$; re-plotted
 482 based on data from (You and Mysore 2020); Methods). Here, we analyzed that dataset with the conditional
 483 accuracy analysis to investigate whether an incongruent flanker affected the sensory encoding stage or the
 484 STM-dependent stage of perceptual dynamics.
 485
 486



487
 488

489 **Figure 4. Incongruent flanker modulates the sensory encoding stage of the conditional accuracy function (CAF).**
 490 (A) Schematic of the flanker task; target grating is always presented at the lower location; a second ‘flanker’ grating
 491 (orthogonal orientation – incongruent flanker, or same orientation – congruent flanker) is presented simultaneously,
 492 and always at the upper location; luminance of flanker is systematically varied (adapted from (You and Mysore 2020)).
 493 All other conventions as in Figure 1. The stimuli were presented for 1s and the response window was 3s. (B) Left
 494 panel: Comparison of performance between trials with incongruent vs. congruent flanker. $p < 0.001$, paired-sample t
 495 test. effect size Hedges’ $g = 1.61$. Right panel: Comparison of median RT between trials with incongruent vs. congruent
 496 flanker. $p = 0.137$, paired-sample t test. effect size Hedges’ $g = -0.176$. Data re-analyzed from You et al (You and Mysore
 497 2020); each line represents data from one mouse ($n = 17$ mice). Data in B-F include only trials with high flanker
 498 luminance (≥ 20.1 cd/m²; see text). (C) CAFs of the sensory encoding stage; Blue: trials with congruent flanker; red:
 499 trials with incongruent flanker; histograms; RT distributions. (D) Key parameters of CAFs (sensory encoding stage)
 500 for trials with congruent vs. incongruent flanker; a_{peak} (left), slope parameter (middle), and t_{peak} (right). Box plots show
 501 the distribution of bootstrapped estimates (Methods). Effect sizes (congruent – incongruent): a_{peak} : Hedges’ $g = 11.0$;
 502 slope parameter: Hedges’ $g = -1.73$; t_{peak} : Hedges’ $g = 2.08$. Note, the sizes of the boxes in the left and right panels are
 503 similar to the sizes of the circular symbols depicting the medians. (E) CAFs of the STM-dependent stage; data aligned
 504 to stimulus offset. Blue: trials with congruent flanker; red: trials with incongruent flanker. (F) Plots of key parameters
 505 of CAFs (STM-dependent stage) for trials with congruent vs. incongruent flanker; a_{peak} (left), t_{chance} (middle) and t_{decay}
 506 (right). Conventions and statistical methods as in D. a_{peak} : Hedges’ $g = 2.54$; t_{chance} : Hedges’ $g = 2.98$; t_{decay} : Hedges’
 507 $g = 0.175$.

508
 509 To investigate the effect of the flanker on perceptual dynamics, we pooled trials from all mice into two
 510 groups based on their flanker congruency, and sorted the trials based on their RT. Since previous study
 511 (You and Mysore 2020) has demonstrated that the flanker affects performance significantly only when its
 512 luminance is higher than (or equal to) that of the target, here we included only high-luminance trials (trials
 513 with flanker luminance ≥ 20.1 cd/m²). To examine the sensory encoding stage quantitatively, we followed
 514 the approach used in Figure 2 and selected the trials on which mice responded before the stimulus ended
 515 ($RT < 1000$ ms), and aligned them to stimulus onset. Separately, to examine the STM-dependent stage, we
 516 followed the approach used in Figure 3 and selected the trials on which responses were made after the
 517 stimulus ended, and aligned them to stimulus offset.

518
 519 The sensory encoding stage was significantly modulated by flanker congruency (Fig. 4CD). We found that,
 520 the peak conditional accuracy for incongruent trials was significantly lower than that of congruent trials
 521 (Fig. 4D-left; a_{peak} : congruent, median [C.I.] = 87.8 [86.3, 89.6] %, incongruent = 78.5 [76.9, 80.2] %; effect
 522 size (congruent-incongruent) Hedges’ $g = 11.0$), indicating that the presence of a high-luminance
 523 incongruent flanker interfered with the sensory encoding of the target stimulus. While the slope parameter
 524 for incongruent trials remains comparable to that of the congruent trials (Fig. 4D middle; congruent = 11.9
 525 [9.10, 15.5] a.u., incongruent = 15.3 [11.6, 20.6] a.u.; Hedges’ $g = -1.73$), the time to reach peak accuracy
 526 was, however, shorter for incongruent trials (Fig. 4D-right; t_{peak} : congruent = 413 [378, 458] ms,
 527 incongruent = 374 [340, 410] ms; Hedges’ $g = 2.08$), consistent with the lower a_{peak} (Fig. 4D-left).

528
 529 The STM-dependent stage also appeared to be modulated by flanker congruency (Fig. 4EF). Following
 530 stimulus offset, the time at which conditional accuracy dropped to chance was much earlier in incongruent
 531 trials than in congruent trials (Fig. 4F-right; t_{chance} : congruent, median [C.I.] = 2000 [1363, 2000] ms;
 532 incongruent = 1145 [816, 1985] ms; Hedges’ $g = 2.98$). However, this was likely due largely to the lower
 533 peak conditional accuracy for incongruent trials (Fig. 4F-left; a_{peak} : congruent = 84.5 [76.9, 88.6] %;
 534 incongruent = 75.9 [70.1, 82.1] %; Hedges’ $g = 2.54$), as opposed to changes in t_{decay} (Fig. 4F-middle;
 535 congruent = 299 [197, 1086] ms; incongruent = 343 [126, 802] ms; Hedges’ $g = 0.175$), or to the rate of decay
 536 (slope parameter; data not shown, congruent = -1.82 [-10, -1.0] a.u., incongruent = -4.82 [-10.0, -1.60] a.u.;
 537 Hedges’ $g = 0.99$).

538
 539 In sum, we found that the presence of an incongruent flanker interferes the sensory encoding stage but not
 540 the STM-dependent stage of mouse visual decision dynamics.

541

542

543 **Stimulus onset delay modulates RT distribution but not the conditional accuracy function**

544 The components of behavioral performance that we have investigated thus far, namely, overall decision
545 accuracy, RT distribution and conditional accuracy function are related formally in the following way: the
546 overall decision accuracy is the dot product of the conditional accuracy function and RT distribution.

547

548 Our manipulations, thus far, produced changes in the conditional accuracy function predominantly. Here,
549 we wondered whether task parameters could, instead, alter RT distribution, and possibly do so without
550 affecting the conditional accuracy function. To test this, we added a delay between trial initiation and target
551 onset (called stimulus onset delay) in the single stimulus discrimination task. We reasoned that the extent
552 to which mice are unable to adaptively withhold responding could impact the RT distribution.

553

554 We found that adding a stimulus onset delay did alter the RT distribution of mice (Fig. 5A-upper panel).
555 The median RTs, measured relative to trial initiation, showed an increasing trend with delay (one-way
556 ANOVA, $p=0.094$; effect size $\eta^2=0.179$; Pearson's correlation= 0.422 , $p=0.028$). This indicated that mice
557 were able to sense the delayed onset of stimulus and thereby withhold their responses. However, mice were
558 unable to withhold responding for the full duration required. By performing a linear regression (Fig. 5A-
559 upper panel; dashed line), we found that mice were able to withhold their responses for only 39 ms for
560 every 100ms of delay. Separately, this increase in RT for longer delays was accompanied by a trend towards
561 lower decision accuracy (Fig. 5A-lower panel, one-way ANOVA, $p=0.182$; effect size $\eta^2=0.132$; Pearson's
562 correlation= -0.358 , $p=0.067$).

563

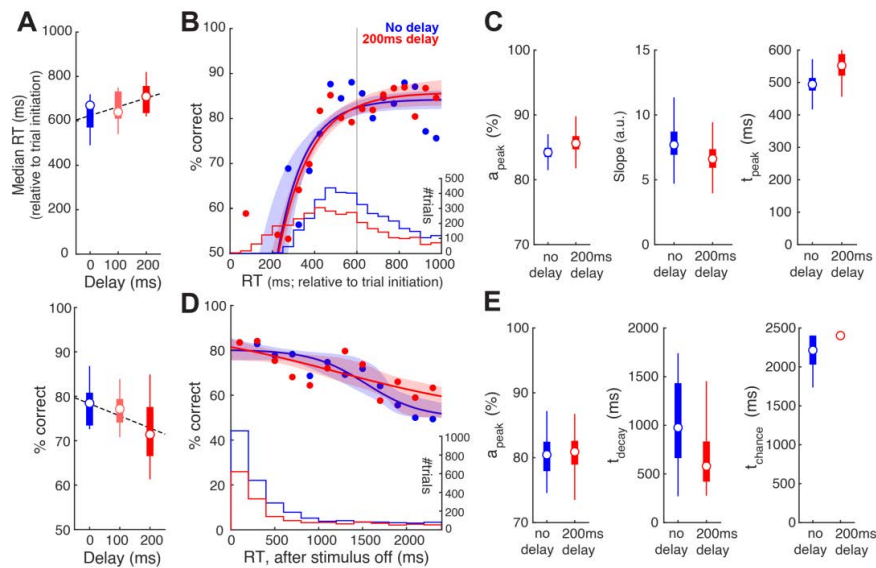
564 By contrast, conditional accuracy analysis revealed no effect of stimulus onset delay either on the sensory
565 encoding stage (Fig. 5BC, a_{peak} : no-delay, median [C.I.] = 84.2 [82.2, 86.4]%, 200ms-delay = 85.6 [82.9,
566 89.2]%, effect size (no-delay - 200ms-delay) Hedges' $g=-1.12$; slope parameter: no-delay = 7.69 [5.82, 10.7]
567 a.u., 200ms-delay = 6.61 [4.63, 8.74] a.u., Hedges' $g=0.264$; t_{peak} : no-delay = 494 [436, 557] ms, 200ms-
568 delay = 552 [476, 680] ms, Hedges' $g=-1.49$), or on the STM-dependent stage (Fig. 5DE, a_{peak} : no-delay,
569 median [C.I.] = 80.5 [75.6, 85.5]%, 200ms-delay = 80.9 [75.6, 84.9]%, Hedges' $g=-0.147$; t_{decay} : no-delay
570 = 976 [332, 1642] ms, 200ms-delay = 580 [319, 1585] ms, Hedges' $g=0.877$; t_{chance} : no-delay = 2214 [1865,
571 2400] ms, 200ms-delay = 2400 [1935, 2400] ms, Hedges' $g=-1.22$).

572

573 Taken together, our results from varying the stimulus onset delay show that changes in RT distribution
574 (and overall decision accuracy) are not necessarily accompanied by changes in the conditional accuracy
575 function. The observed trend of decreased accuracy was accounted for by the fact that with a delay, there
576 were more responses initiated before the sensory encoding was complete, or even before the stimulus was
577 presented (i.e., 'impulsive' responses) (Fig. 5B, histograms). To quantify such impulsivity, we propose an
578 'impulsivity index' (ImpI): $ImpI = 1 - \text{average (duration for which mice withhold responses /duration of}$
579 $\text{the delay})$. Higher positive values of this index indicate greater impulsivity, with $ImpI=1$ indicating a
580 complete inability to withhold responding in the face of stimulus delays ('maximally' impulsive). In the
581 case of our mice, $ImpI$ is ~ 0.6 .

582

583



584
 585 **Figure 5. Stimulus onset delay modulates RT distribution but not the conditional accuracy function.** (A) *Upper:*
 586 Plot of median RT, measured relative to train initiation, against stimulus onset delay (n=9 mice; p=0.094, 1-way
 587 ANOVA; effect size $\eta^2=0.179$; Pearson's correlation=0.422, p=0.028). Dashed line: Linear regression on RTs. *Lower:*
 588 Plot of response accuracy against stimulus onset delay (p=0.182, 1-way ANOVA; effect size $\eta^2=0.132$; Pearson's
 589 correlation=-0.358, p=0.067). (B) Conditional accuracy functions of the sensory encoding stage; Blue: trials with no
 590 delay; red: trials with 200ms delay; shaded bands: bootstrap confidence intervals (95%); confidence intervals overlap
 591 for the two datasets. Histograms: RT distributions. Grey vertical line: stimulus offset. (C) Key parameters of the CAF
 592 (sensory encoding stage) for trials with no delay vs. trials with 200ms delay. Box plots show the distribution of the
 593 bootstrapped estimates. (D) Conditional accuracy functions of the STM-dependent stage. Conventions as in B. (E)
 594 Key parameters of the CAF (STM-dependent stage) for trials with no delay vs. trials with 200ms delay. Conventions
 595 as in C.

596 See also Fig. 5-1.

597 DISCUSSION

598
 599 In this study, we quantify two distinct stages in the temporal dynamics of visual perceptual decisions in
 600 mice. First, a sensory encoding stage that is subject to the speed-accuracy tradeoff, and then, a short-term
 601 memory dependent stage in which decision performance decays once the stimulus disappears. We also
 602 demonstrate that the conditional accuracy function and the RT distribution can be affected independently
 603 by experimental manipulations. Whereas stimulus size, luminance and presence of a foil modulate the
 604 conditional accuracy function with minimal changes to the RT distribution, stimulus onset asynchrony
 605 modulates the RT distribution without changes to the conditional accuracy function. Additionally, our
 606 results yield numerical estimates of fundamental psychophysical constants of visual perceptual decision-
 607 making in mice. Taken together, this study establishes a quantitative platform for future work dissecting
 608 neural circuit underpinnings of the dynamics of visually guided decision-making in mice.
 609

610 Estimates of time constants of the dynamics of visual perceptual decision-making in mice

611
 612 Our results yielded numerical estimates of the duration of sensory encoding (i.e., the window of temporal
 613 integration) as 200-320 ms across stimulus size and luminance in mice (Fig. 2). This estimate is similar to
 614 that in humans: the internal representation of a visual stimulus is thought to be constructed within the first
 615 200-300 ms of stimulus presentation (Shibuya and Bundesen 1988, Busey and Loftus 1994, Vogel,
 616 Woodman et al. 2006, Bays, Gorgoraptis et al. 2011). On the other hand, we also obtained an estimate of

617 the duration of STM as 1700 ms. This constituted the period starting from stimulus offset to the last instant
618 at which responses that are better than chance were *initiated* (Fig. 3D; $t_{\text{chance}} - t_{\text{delay}} = \sim 1700$ ms). This
619 duration does not necessarily represent just the maintenance of visual stimulus information in STM, it could
620 also represent maintenance of information about the motor response associated with the stimulus (and likely,
621 a combination of the two). Notably, our estimate of the duration of viability of the labile internal
622 representation in mice falls in the same range as has been reported from human studies (Sperling 1960,
623 Posner and Keele 1967, Phillips and Baddeley 1971).

624
625 We have interpreted the decay in performance following stimulus offset as being due to loss of information
626 in STM. A potential confounding factor to this interpretation is differences in the internal state of the animal
627 – in selective attention, or more generally, task engagement. It is possible, for instance, that all the trials
628 with longer RTs represent those in which mice did not pay attention to the stimulus (or more generally,
629 were disengaged from the task), thereby being associated with lower accuracy. We believe this unlikely
630 because attention/engagement was not varied systematically, here (unlike in the flanker task, Fig. 4). Even
631 if loss of attention or engagement were a factor, any improvements in conditional accuracy due to increased
632 attentiveness or engagement would only lengthen STM. From this perspective, our estimate of 1700 ms
633 serves as a *lower bound* for the duration of STM.

634
635 This estimate of 1700 ms also represents a lower bound for working memory (WM). Whereas STM refers
636 to the retention of information even when it is not accessible from the environment, WM refers additionally
637 to the ability to manipulate this information and protect it from interference (Cowan 2008, Postle and
638 Pasternak 2009). WM can be lengthened with training. For instance, in tasks that require animals hold
639 information over an enforced delay period before responding, it has been reported that mice can learn to
640 perform well with delay periods up to 5 sec (Liu, Gu et al. 2014). Here, by allowing the natural evolution
641 of the dynamics of decision-making to occur without an imposed delay period, we were able to estimate
642 the ‘intrinsic’ (lower bound for the) duration of STM.

643
644 **Estimates of the operating range of stimulus features for visual perceptual decision-making in mice**
645 This study also yielded estimates for the range of values of various stimulus features within which mice are
646 able to discriminate the visual target. The smallest stimulus size and lowest luminance (tested) at which
647 mice were able to discriminate orientation above chance were 25° and 2.00 cd/m^2 , with mice performing at
648 $> 80\%$ accuracy for most luminance values at that smallest size. The shortest stimulus that mice are able to
649 discriminate above chance was $\leq 100\text{ms}$ (Fig. 3A). Further, based on the x-intercept of the CAF in sensory
650 encoding stage (median [C.I.] = $236 [215, 253]$ ms, pooling all trials of various sizes and luminance from
651 Fig. 2), we were able to refine this estimate to be $\leq 53\text{ms}$ (conservatively, after subtracting $t_{\text{delay}} = \sim 200$ ms).
652 This is consistent to the estimation (40-80 ms) from a previous study based on visual cortical activity
653 (Resulaj, Ruediger et al. 2018). In a subgroup of animals ($n=3$), we tested if mice are able to discriminate
654 orientation of the target stimulus (25° , 0.1 cpd , 16.2 cd/m^2) when it was 50 ms long. Two out of the three
655 mice showed a response accuracy higher than chance (accuracy = 57.9% , 210 correct out of 363 trials,
656 $p=0.002$, binomial test; and 55.6% , 143/257, $p=0.040$, respectively), consistent with this refined estimate.
657 These findings that mice are able to discriminate visual stimuli in demanding sensory contexts suggest that
658 the visual perceptual abilities of mice may be underrated.

659
660 The best discrimination performance reported in mice (accuracies $> 90\%$) have typically been obtained
661 using large, often full-field, grating stimuli (Andermann, Kerlin et al. 2010, Long, Jiang et al. 2015). In our
662 single target discrimination task, the best performance ranged lower, between 75-90% (Fig. 1C), consistent
663 with our use of ‘small’ stimuli (relative to those typically used in mouse vision studies (Prusky, West et al.
664 2000, Prusky and Douglas 2004, Wong and Brown 2006, Busse, Ayaz et al. 2011, Long, Jiang et al. 2015))
665 and the lower visual acuity of mice. Indeed, in our pilot study, the performance plateaued at $\sim 93\%$ for a
666 stimulus size $\geq 45^\circ$ (Fig. 1-ICD). These results suggest that full-field stimuli may be effectively replaced
667 by 45° stimuli to achieve best performance levels.

668
669 The best discrimination performance exhibited a dip at the highest luminance (Fig. 1C). This is potentially
670 well accounted for by signal saturation: because the visual system adapts to the relevant range of stimulus
671 luminance for best encoding (Ohzawa, Sclar et al. 1982), the interleaved presentation of stimuli with
672 different luminance can render the maximum-luminance stimulus unfavorable because of signal saturation
673 (Long, Jiang et al. 2015). Consistent with this idea, when the maximum-luminance stimulus (25° , 0.1cpd,
674 130 cd/m^2) was presented *alone* in block design (Fig. 1-1C, the green box at the left most, group median
675 [C.I.] = 85.7 [77.6, 92.1] %), response accuracy was nominally higher than when it was presented
676 interleaved with stimuli of varying luminance (Fig. 1C, the red box at the right most, group median [C.I.]
677 = 79.7 [61.9, 91.9] %). These results indicate that a good upper bound for stimulus luminance in mouse
678 experiments may be $\sim 34 \text{ cd/m}^2$.

679 **Stimulus and task parameters modulate perceptual performance through a variety of mechanisms**

680 Increase in stimulus size and luminance both improved the overall discrimination performance of mice (Fig.
681 1). However, analysis of conditional accuracy revealed that whereas increasing each increased the peak
682 conditional accuracy (a_{peak}), only increasing the stimulus luminance increased the slope of the CAF and
683 resulted in a shorter t_{peak} (Fig. 2). We propose that these differences in the CAF reflect differential
684 mechanisms at one or more levels of the underlying sensory processing. Specifically, in our experiments,
685 varying stimulus luminance (through varying the intensity of just the bright phase of the grating) also varied
686 stimulus contrast (relative to the dark background). On the other hand, increasing stimulus size increased
687 the total luminance without affecting contrast. Consequently, differential activation of lateral inhibitory
688 mechanisms for spatial contrast may account for the observed differences in CAFs. Separately, whereas
689 increasing stimulus size and luminance both increase the total number of photons impinging on the retina,
690 increasing stimulus size would activate a broader spatial distribution of photoreceptors (at a fixed signal-
691 to-noise ratio), while increasing stimulus luminance would cause a largely fixed group of photoreceptors to
692 receive a higher density of photons (and higher signal-to-noise ratio). Consequently, differential
693 mechanisms of sensory integration (of the two) may also account for the observed differences in CAFs.

694
695 Separately, manipulating attention (by presenting a flanker) and manipulating the stimulus onset
696 asynchrony both caused a reduction in response accuracy (Fig.4B, 5A-lower panel). However, again, the
697 analysis of conditional accuracy suggests that the mechanisms underlying the two are different: the capture
698 of attention by the flanker interferes with the target's sensory encoding, whereas adding a pre-stimulus
699 onset delay results in change of the RT distribution without affecting the CAF.

700
701 Taken together, our results demonstrate that although manipulating stimulus parameters or experimental
702 conditions may induce seemingly similar changes in perceptual performance (overall accuracy), their
703 underlying mechanisms could be different. The conditional accuracy analysis serves as an informative tool
704 to explore these mechanisms and to understand the dynamics of perceptual decision making.

705 **Qualitative differences between stimulus features as well as between task-difficulties**

706
707 Across the various tasks and stimulus conditions that we studied here in mice, the sensory encoding stage
708 ended rapidly, around 300ms. However, in a recent study in which rats discriminated the direction of
709 motion of a patch of random dots, the sensory encoding stage continued through at least 1.5 s (the longest
710 RT bin reported (Shevinsky and Reinagel 2019)). We propose that this difference in the duration of
711 sensory encoding may be due to fundamentally different nature of stimulus features used in these two
712 studies. Consistent with this proposal, a study on human visual psychophysics (Burr and Santoro 2001)
713 has reported a temporal integration window of 200-300ms when stimulus contrast of a patch of random
714 dots was varied (similar to our results in mice), but a substantially longer integration window of 3s when
715 their motion coherence levels were varied (similar to the above-mentioned results in rats).

716
717

718 Separately, our results also highlight that ‘task difficulty’ may be altered in qualitatively different ways,
 719 producing distinct outcomes on behavior. In the literature, task difficulty is often increased by making target
 720 stimuli more ambiguous or by introducing distracters (which we did also). Such manipulations often cause
 721 subjects (animals) to respond slower, allowing them time to gather more information to produce better
 722 performance (which we found, as well). However, when we shortened stimulus duration, which can
 723 plausibly be considered to also increase task difficulty, we found the opposite result – mice responded faster
 724 as the target stimulus became shorter (Fig. 3B). This potentially counter-intuitive effect (faster RTs for a
 725 ‘more difficult’ task) is explained well by the conditional accuracy analysis (Fig. 3C). Whereas shortening
 726 the stimulus duration makes the task more difficult, responding more slowly to shorter stimuli does not
 727 grant a perceptual benefit to the animals: once the stimulus has disappeared, withholding responses for
 728 longer would only increase the risk of losing information owing to memory decay. In other words, short
 729 stimuli impose a ‘time pressure’ on animals to make decisions quickly. Thus, task difficulty may be altered
 730 in qualitatively different ways, with distinct behavioral effects.
 731

732 **Optimal sensory sampling during visual perceptual decision-making in mice**

733 An intriguing observation in our study is that across tasks, the peak of RT distribution (the RT bin with the
 734 largest number of trials) always seemed to occur around t_{peak} (Fig. 2AC, 4C). Since the RT distribution can
 735 vary independently of the conditional accuracy function (as demonstrated in Fig. 5), there is *no priori* reason
 736 that the peak of RT distribution and the t_{peak} must change together. We propose that responding with RTs
 737 close to t_{peak} may be an optimal behavioral strategy for the mice. As indicated by the conditional accuracy
 738 function, mouse response accuracy increased as RT increased until it reached a plateau at t_{peak} . Responding
 739 earlier than t_{peak} , therefore, would sacrifice accuracy, while responding later than t_{peak} would needlessly delay
 740 response (reducing the reward rate). Consequently, responding with the peak of RT distribution being equal
 741 to t_{peak} would be optimal. Testing this optimality hypothesis would require future experiments to manipulate
 742 the temporal integration window (t_{peak}) substantially (much more than the 40 ms - 120 ms change we find
 743 in Figs. 2BD, 4D) – for instance, by manipulating stimulus coherence (Burr and Santoro 2001) or the
 744 volatility of environment (Piet, El Hady et al. 2018), and to ask if this is accompanied by a commensurate
 745 shift in peak RT.
 746
 747

748 **EXTENDED DATA**

749 Extended data (Fig. 1-1, 2-1, 2-2, 3-1, and 5-1) and legends are included.
 750
 751

752 **REFERENCES**

- 753 Andermann, M. L., A. M. Kerlin and R. C. Reid (2010). "Chronic cellular imaging of mouse visual cortex during
 754 operant behavior and passive viewing." Front Cell Neurosci **4**: 3.
 755 Barrouillet, P. and V. Camos (2012). "As time goes by: Temporal constraints in working memory." Current
 756 Directions in Psychological Science **21**(6): 413-419.
 757 Bays, P. M., N. Gorgoraptis, N. Wee, L. Marshall and M. Husain (2011). "Temporal dynamics of encoding, storage,
 758 and reallocation of visual working memory." Journal of vision **11**(10): 6-6.
 759 Brown, J. (1958). "Some tests of the decay theory of immediate memory." Quarterly Journal of Experimental
 760 Psychology **10**(1): 12-21.
 761 Burgess, C. P., A. Lak, N. A. Steinmetz, P. Zatzka-Haas, C. Bai Reddy, E. A. K. Jacobs, J. F. Linden, J. J. Paton, A.
 762 Ranson, S. Schroder, S. Soares, M. J. Wells, L. E. Wool, K. D. Harris and M. Carandini (2017). "High-Yield
 763 Methods for Accurate Two-Alternative Visual Psychophysics in Head-Fixed Mice." Cell Rep **20**(10): 2513-2524.
 764 Burr, D. C. and L. Santoro (2001). "Temporal integration of optic flow, measured by contrast and coherence
 765 thresholds." Vision research **41**(15): 1891-1899.
 766 Busey, T. A. and G. R. Loftus (1994). "Sensory and cognitive components of visual information acquisition."
 767 Psychological Review **101**(3): 446.
 768 Busse, L., A. Ayaz, N. T. Dhruv, S. Katzner, A. B. Saleem, M. L. Scholvinck, A. D. Zaharia and M. Carandini
 769 (2011). "The detection of visual contrast in the behaving mouse." J Neurosci **31**(31): 11351-11361.

- 770 Carandini, M. and A. K. Churchland (2013). "Probing perceptual decisions in rodents." Nature neuroscience **16**(7):
771 824.
- 772 Coltheart, M. (1980). "Iconic memory and visible persistence." Perception & psychophysics **27**(3): 183-228.
- 773 Cowan, N. (2008). "What are the differences between long-term, short-term, and working memory?" Progress in
774 brain research **169**: 323-338.
- 775 Dick, A. (1974). "Iconic memory and its relation to perceptual processing and other memory mechanisms."
776 Perception & Psychophysics **16**(3): 575-596.
- 777 Eriksen, B. A. and C. W. Eriksen (1974). "Effects of noise letters upon the identification of a target letter in a
778 nonsearch task." Perception & Psychophysics **16**(1): 143-149.
- 779 Fan, J., B. D. McCandliss, T. Sommer, A. Raz and M. I. Posner (2002). "Testing the efficiency and independence of
780 attentional networks." J Cogn Neurosci **14**(3): 340-347.
- 781 Glickfeld, L. L., M. H. Histed and J. H. Maunsell (2013). "Mouse primary visual cortex is used to detect both
782 orientation and contrast changes." J Neurosci **33**(50): 19416-19422.
- 783 Glickfeld, L. L., R. C. Reid and M. L. Andermann (2014). "A mouse model of higher visual cortical function."
784 Current opinion in neurobiology **24**: 28-33.
- 785 Gold, J. M., R. F. Murray, A. B. Sekuler, P. J. Bennett and R. Sekuler (2005). "Visual memory decay is
786 deterministic." Psychological Science **16**(10): 769-774.
- 787 Guo, Z. V., S. A. Hires, N. Li, D. H. O'Connor, T. Komiyama, E. Ophir, D. Huber, C. Bonardi, K. Morandell, D.
788 Gutnisky, S. Peron, N. L. Xu, J. Cox and K. Svoboda (2014). "Procedures for behavioral experiments in head-fixed
789 mice." PLoS One **9**(2): e88678.
- 790 Heitz, R. P. (2014). "The speed-accuracy tradeoff: history, physiology, methodology, and behavior." Frontiers in
791 neuroscience **8**: 150.
- 792 Hentschke, H. and M. C. Stüttgen (2011). "Computation of measures of effect size for neuroscience data sets."
793 European Journal of Neuroscience **34**(12): 1887-1894.
- 794 Histed, M. H., L. A. Carvalho and J. H. Maunsell (2012). "Psychophysical measurement of contrast sensitivity in the
795 behaving mouse." J Neurophysiol **107**(3): 758-765.
- 796 Histed, M. H. and J. H. Maunsell (2014). "Cortical neural populations can guide behavior by integrating inputs
797 linearly, independent of synchrony." Proceedings of the National Academy of Sciences **111**(1): E178-E187.
- 798 Huberman, A. D. and C. M. Niell (2011). "What can mice tell us about how vision works?" Trends Neurosci **34**(9):
799 464-473.
- 800 Liu, D., X. Gu, J. Zhu, X. Zhang, Z. Han, W. Yan, Q. Cheng, J. Hao, H. Fan, R. Hou, Z. Chen, Y. Chen and C. T. Li
801 (2014). "Medial prefrontal activity during delay period contributes to learning of a working memory task." Science
802 **346**(6208): 458-463.
- 803 Long, M., W. Jiang, D. Liu and H. Yao (2015). "Contrast-dependent orientation discrimination in the mouse." Sci
804 Rep **5**: 15830.
- 805 Mar, A. C., A. E. Horner, S. R. Nilsson, J. Alsio, B. A. Kent, C. H. Kim, A. Holmes, L. M. Saksida and T. J. Bussey
806 (2013). "The touchscreen operant platform for assessing executive function in rats and mice." Nat Protoc **8**(10):
807 1985-2005.
- 808 McElree, B. and B. A. Doshier (1989). "Serial position and set size in short-term memory: the time course of
809 recognition." Journal of Experimental Psychology: General **118**(4): 346.
- 810 Meier, P., E. Flister and P. Reinagel (2011). "Collinear features impair visual detection by rats." Journal of vision
811 **11**(3): 22-22.
- 812 Miller, J. (1991). "The flanker compatibility effect as a function of visual angle, attentional focus, visual transients,
813 and perceptual load: a search for boundary conditions." Percept Psychophys **49**(3): 270-288.
- 814 Nomura, Y., S. Ikuta, S. Yokota, J. Mita, M. Oikawa, H. Matsushima, A. Amano, K. Shimonomura, Y. Seya and C.
815 Koike (2019). "Evaluation of critical flicker-fusion frequency measurement methods using a touchscreen-based
816 visual temporal discrimination task in the behaving mouse." Neuroscience research **148**: 28-33.
- 817 Ohzawa, I., G. Sclar and R. D. Freeman (1982). "Contrast gain control in the cat visual cortex." Nature **298**(5871):
818 266-268.
- 819 Phillips, W. and A. Baddeley (1971). "Reaction time and short-term visual memory." Psychonomic Science **22**(2):
820 73-74.
- 821 Piet, A. T., A. El Hady and C. D. Brody (2018). "Rats adopt the optimal timescale for evidence integration in a
822 dynamic environment." Nature communications **9**(1): 1-12.
- 823 Posner, M. I. and S. W. Keele (1967). "Decay of visual information from a single letter." Science **158**(3797): 137-
824 139.

- 825 Postle, B. and T. Pasternak (2009). "Short term and working memory." Encyclopedia of Neuroscience. San Diego,
826 CA: Elsevier: 783-789.
- 827 Prusky, G. T. and R. M. Douglas (2004). "Characterization of mouse cortical spatial vision." Vision Res **44**(28):
828 3411-3418.
- 829 Prusky, G. T., P. W. West and R. M. Douglas (2000). "Behavioral assessment of visual acuity in mice and rats."
830 Vision Res **40**(16): 2201-2209.
- 831 Ratcliff, R. (1978). "A theory of memory retrieval." Psychological Review **85**(2): 59-108.
- 832 Ratcliff, R., P. L. Smith, S. D. Brown and G. McKoon (2016). "Diffusion Decision Model: Current Issues and
833 History." Trends Cogn Sci **20**(4): 260-281.
- 834 Resulaj, A., S. Ruediger, S. R. Olsen and M. Scanziani (2018). "First spikes in visual cortex enable perceptual
835 discrimination." Elife **7**: e34044.
- 836 Ricker, T. J., E. Vergauwe and N. Cowan (2016). "Decay theory of immediate memory: From Brown (1958) to
837 today (2014)." The Quarterly Journal of Experimental Psychology **69**(10): 1969-1995.
- 838 Seabrook, T. A., T. J. Burbridge, M. C. Crair and A. D. Huberman (2017). "Architecture, function, and assembly of
839 the mouse visual system." Annual review of neuroscience **40**: 499-538.
- 840 Shevinsky, C. A. and P. Reinagel (2019). "The interaction between elapsed time and decision accuracy differs
841 between humans and rats." Frontiers in neuroscience **13**: 1211.
- 842 Shibuya, H. and C. Bundesen (1988). "Visual selection from multielement displays: measuring and modeling effects
843 of exposure duration." Journal of Experimental Psychology: Human Perception and Performance **14**(4): 591.
- 844 Siegel, M., A. K. Engel and T. H. Donner (2011). "Cortical network dynamics of perceptual decision-making in the
845 human brain." Frontiers in human neuroscience **5**: 21.
- 846 Smith, P. L. and R. Ratcliff (2009). "An integrated theory of attention and decision making in visual signal
847 detection." Psychol Rev **116**(2): 283-317.
- 848 Speed, A., J. Del Rosario, N. Mikail and B. Haider (2020). "Spatial attention enhances network, cellular and
849 subthreshold responses in mouse visual cortex." Nature communications **11**(1): 1-11.
- 850 Sperling, G. (1960). "The information available in brief visual presentations." Psychological monographs: General
851 and applied **74**(11): 1.
- 852 Stanford, T. R., S. Shankar, D. P. Massoglia, M. G. Costello and E. Salinas (2010). "Perceptual decision making in
853 less than 30 milliseconds." Nature neuroscience **13**(3): 379.
- 854 Steinemann, N. A., R. G. O'Connell and S. P. Kelly (2018). "Decisions are expedited through multiple neural
855 adjustments spanning the sensorimotor hierarchy." Nature communications **9**(1): 1-13.
- 856 Thura, D. and P. Cisek (2014). "Deliberation and commitment in the premotor and primary motor cortex during
857 dynamic decision making." Neuron **81**(6): 1401-1416.
- 858 Uchida, N., A. Kepecs and Z. F. Mainen (2006). "Seeing at a glance, smelling in a whiff: rapid forms of perceptual
859 decision making." Nature Reviews Neuroscience **7**(6): 485-491.
- 860 Umino, Y., R. Pasquale and E. Solessio (2018). "Visual temporal contrast sensitivity in the behaving mouse shares
861 fundamental properties with human psychophysics." eNeuro **5**(4).
- 862 Vogel, E. K., G. F. Woodman and S. J. Luck (2006). "The time course of consolidation in visual working memory."
863 Journal of Experimental Psychology: Human Perception and Performance **32**(6): 1436.
- 864 Voss, A., M. Nagler and V. Lerche (2013). "Diffusion models in experimental psychology: a practical introduction."
865 Exp Psychol **60**(6): 385-402.
- 866 Voss, A., J. Voss and V. Lerche (2015). "Assessing cognitive processes with diffusion model analyses: a tutorial
867 based on fast-dm-30." Front Psychol **6**: 336.
- 868 Wang, L. and R. J. Krauzlis (2018). "Visual Selective Attention in Mice." Curr Biol **28**(5): 676-685.e674.
- 869 Whitney, D. and D. M. Levi (2011). "Visual crowding: a fundamental limit on conscious perception and object
870 recognition." Trends Cogn Sci **15**(4): 160-168.
- 871 Wickelgren, W. A. (1977). "Speed-accuracy tradeoff and information processing dynamics." Acta psychologica
872 **41**(1): 67-85.
- 873 Wilming, N., P. R. Murphy, F. Meyniel and T. H. Donner (2020). "Large-scale dynamics of perceptual decision
874 information across human cortex." Nature communications **11**(1): 1-14.
- 875 Wong, A. A. and R. E. Brown (2006). "Visual detection, pattern discrimination and visual acuity in 14 strains of
876 mice." Genes Brain Behav **5**(5): 389-403.
- 877 Yang, Y., M. DeWeese, G. Otazu and A. Zador (2008). "Millisecond-scale differences in neural activity in auditory
878 cortex can drive decisions." Nature Precedings: 1-1.
- 879 You, W.-K. and S. P. Mysore (2020). "Endogenous and exogenous control of visuospatial selective attention in
880 freely behaving mice." Nature Communications **11**(1): 1-14.

881 Zariwala, H. A., A. Kepecs, N. Uchida, J. Hirokawa and Z. F. Mainen (2013). "The limits of deliberation in a
882 perceptual decision task." Neuron **78**(2): 339-351.
883 Zhang, W. and S. J. Luck (2009). "Sudden death and gradual decay in visual working memory." Psychological
884 science **20**(4): 423-428.

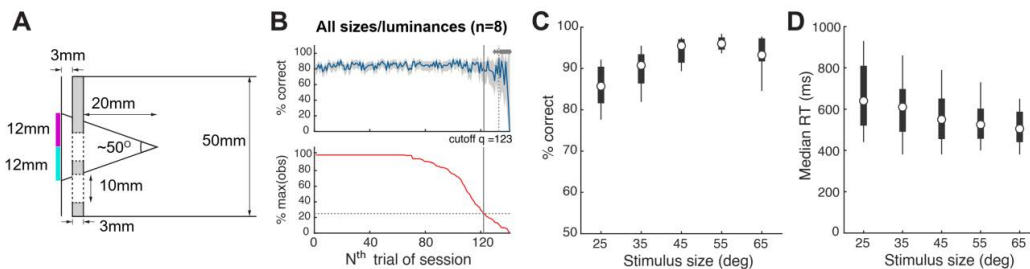
885

886

887 **Extended Data**

888

889



890

891

Figure 1-1. Extended data for Figure 1.

892

893

894

895

896

897

898

899

900

901

902

903

904

905

906

907

908

909

910

911

912

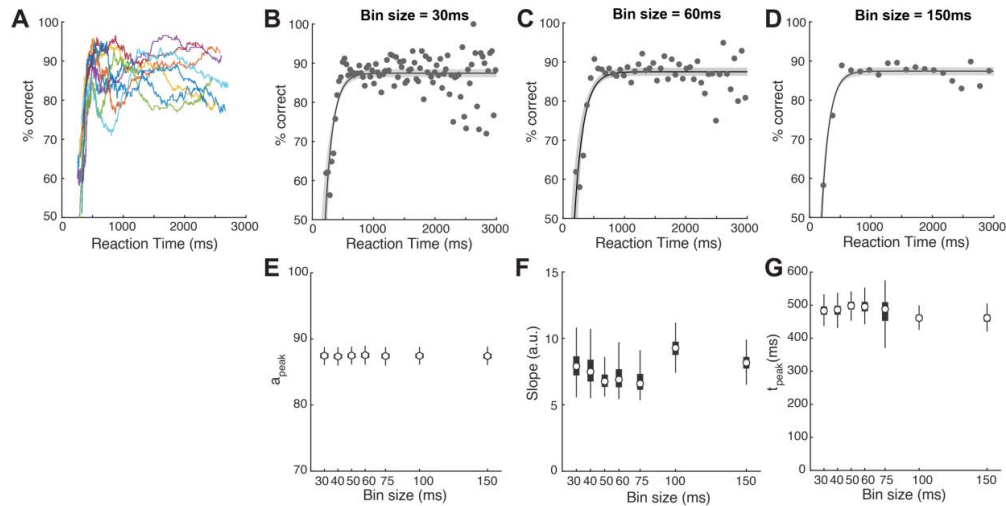
913

914

915

916

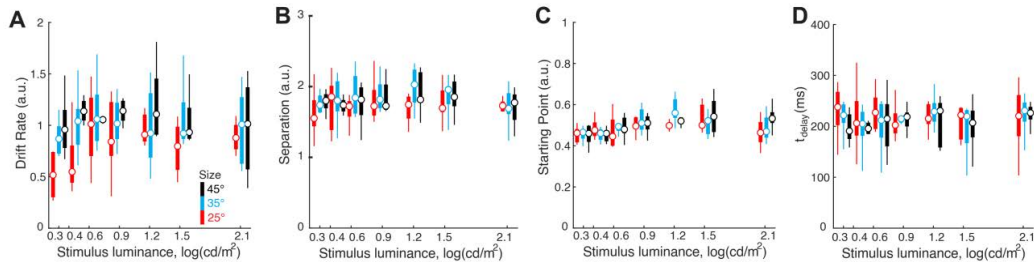
917



918
919
920
921
922
923
924
925
926
927
928
929
930

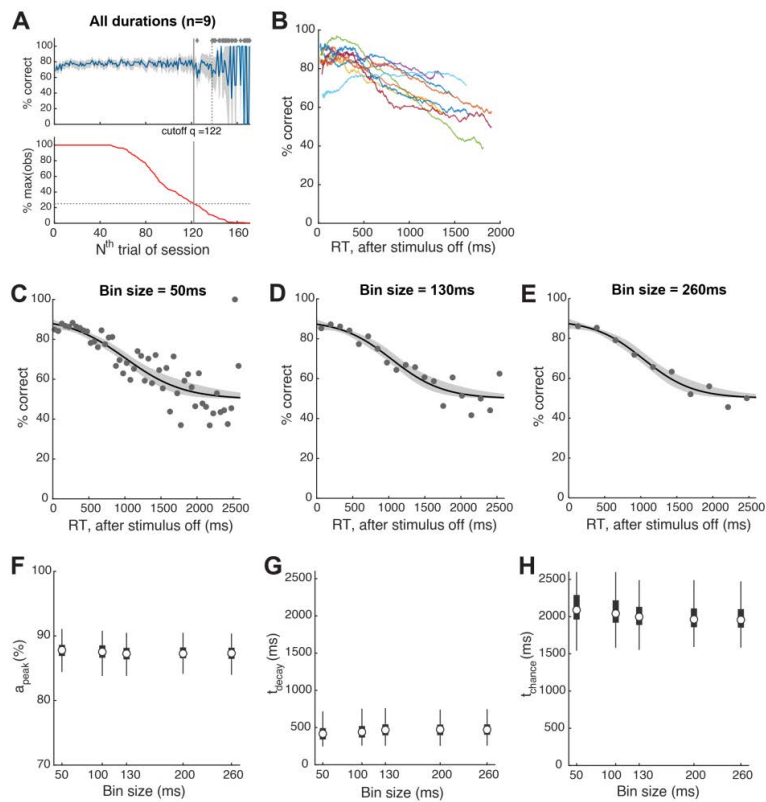
Figure 2-1. Extended data for Figure 2: CAFs of individual mice and effect of bin size.

(A) The general pattern of conditional accuracy curves across mice. Each color represents one single mouse. Each curve was generated by pooling all trials (of various stimulus size and luminance) from one mouse, sort the trials by RT, and then do a moving average (window size = 200 trials) to plot the mean accuracy (y) at mean RT (x) of the time window. (B-D) Fitting of the conditional accuracy function (CAF) in various bin sizes. (B) Bin size = 30ms; (C) Bin size = 60ms; (D) Bin size = 150ms; (E-G) Estimates of the quantitative metrics of the CAF in various bin sizes. (E) peak conditional accuracy (a_{peak}); (F) slope parameter; and (G) time to reach peak conditional accuracy (t_{peak}).



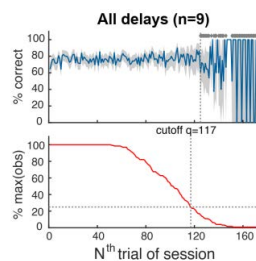
931
932
933
934
935
936
937
938
939

Figure 2-2. Extended data for Figure 2: Estimates of all four parameters of the drift diffusion model. (A) Drift rate; 2-way ANOVA, $p=0.028$ (luminance), $p<0.001$ (size), $p=0.767$ (interaction). **(B)** Boundary separation; 2-way ANOVA, $p=0.171$ (luminance), $p=0.026$ (size), $p=0.953$ (interaction). **(C)** Starting point; 2-way ANOVA, $p<0.001$ (luminance), $p=0.325$ (size), $p=0.098$ (interaction). **(D)** t_{delay} ; 2-way ANOVA, $p=0.523$ (luminance), $p=0.308$ (size), $p=0.931$ (interaction).



940
941
942
943
944
945
946
947
948
949
950
951
952

Figure 3-1. Extended data for Figure 3: CAFs of individual mice and effect of bin size. (A) Identification of trials towards the end of the 30 min behavioral sessions that corresponded to animals being poorly engaged in the task (Methods); conventions identical to those in Fig. 1-1B. (B) The general pattern of conditional accuracy curves across mice. Each color represents one single mouse. Each curve was generated by pooling all trials (of various stimulus size and luminance) from one mouse, sort the trials by RT, and then do a moving average (window size = 200 trials) to plot the mean accuracy (y) at mean RT (x) of the time window. (C-E) Fitting of the conditional accuracy function (CAF) in various bin sizes. (C) Bin size = 50ms; (D) Bin size = 130ms; (E) Bin size = 260ms; (F-H) Estimates of the quantitative metrics of the CAF in various bin sizes. (F) peak conditional accuracy (a_{peak}); (G) the time at which conditional accuracy started to decay (t_{decay}); and (H) the time at which conditional accuracy fell to the chance level (t_{chance}).



953
954
955
956
957
958
959
960

Figure 5-1. Extended data for stimulus onset delay experiment.

Identification of trials towards the end of the 30 min behavioral sessions that corresponded to animals being poorly engaged in the task (Methods). All conventions are as in Fig. 1-1B. Based on these data, all trials above 116 of each behavioral session of this experiment were dropped from analysis. Results in Fig.5 are based on data from trials 1-116 from each behavioral session.